How to cite: *Angew. Chem. Int. Ed.* **2023**, *62*, e202307091
doi.org/10.1002/anie.202307091

EPR Spectroscopy

Time-Resolved Mn^{2+}–NO and NO–NO Distance Measurements Reveal That Catalytic Asymmetry Regulates Alternating Access in an ABC Transporter**

Michael Rudolph, Robert Tampé, and Benesh Joseph**

Abstract: ATP-binding cassette (ABC) transporters shuttle diverse substrates across biological membranes. Transport is often achieved through a transition between an inward-facing (IF) and an outward-facing (OF) conformation of the transmembrane domains (TMDs). Asymmetric nucleotide-binding sites (NBSs) are present among several ABC subfamilies and their functional role remains elusive. Here we addressed this question using concomitant NO–NO, Mn^{2+}–NO, and Mn^{2+}–Mn^{2+} pulsed electron–electron double-resonance spectroscopy of TmrAB in a time-resolved manner. This type-IV ABC transporter undergoes a reversible transition in the presence of ATP with a significantly faster forward transition. The impaired degenerate NBS stably binds Mn^{2+}–ATP, and Mn^{2+} is preferentially released at the active consensus NBS. ATP hydrolysis at the consensus NBS considerably accelerates the reverse transition. Both NBSs fully open during each conformational cycle and the degenerate NBS may regulate the kinetics of this process.

Introduction

Endogenous Mn^{2+} centers can provide structural information for membrane protein complexes when combined with electron spin resonance (ESR) spectroscopy.[1] Here we used Mg^{2+}–to–Mn^{2+} substitution combined with nitroxide labeling to perform time-resolved pulsed dipolar ESR spectroscopy of the ATP-binding cassette (ABC) exporter TmrAB. ABC transporters play a crucial role in cellular physiology by transporting a large variety of substrates, including lipids, peptides, vitamins, and xenobiotics across cell membranes.[2] Despite the functional diversity, their general architecture consists of two nucleotide-binding domains (NBDs) coupled with two transmembrane domains (TMDs). The NBDs constitute two nucleotide-binding sites (NBSs) where ATP binding and hydrolysis takes place, which are directly coupled with conformational changes of the TMDs to enable a productive transport cycle.[3]

TmrAB is a heterodimeric type IV ABC transporter isolated from *Thermus thermophilus*.[4] It is a model system for the human transporter associated with antigen processing (TAP1/2) and can restore antigen presentation in TAP-deficient human cells.[5] A series of eight different cryo-EM structures has been solved, thereby making TmrAB an ideal model system for mechanistic investigations.[6] In TmrAB, deviation from the conserved sequence significantly reduces the ATPase activity at one of the NBSs (called as degenerate NBS, d-NBS). The catalytic glutamate at the consensus NBS (c-NBS) is replaced by an aspartate at the d-NBS. The presence of such asymmetric NBSs is a general blueprint among many ABC exporters including 21 out of 29 human heterodimeric ABC proteins.[7] An asymmetric response of the NBSs has been suggested to be relevant even for transporters having two functional ATPase sites.[8] The sequence of the degenerate NBS has been evolutionarily conserved, suggesting that the catalytic asymmetry might be associated with a new function.

Several ABC exporters with asymmetric NBSs were structurally characterized.[7a,9] While the functional relevance of asymmetric NBSs remains elusive, it is generally accepted that it would lead to substantial differences in the mechanistic details.[10] In the transport model for type IV ABC transporters, the IF-to-OF transition (denoted as forward transition) involves ATP binding at the two NBSs and subsequent opening of the TMDs to the OF conformation (in which the substrate is released). However, the OF-to-IF transition (denoted as reverse transition) might substantially differ between exporters with symmetric or asymmetric NBSs. Though the exact role for a d-NBS is unclear, indirect evidences suggest that ATP might act as a glue to keep it in a closed conformation over several transport cycles.[11] A direct observation of nucleotide interaction at the individual NBSs and the related effects on the TMDs is required to elucidate the role of catalytic asymmetry in regulating the conformational cycle and substrate translocation.

[*] M. Rudolph, Prof. Dr. B. Joseph
Department of Physics, Freie Universität Berlin
Arnimallee 14, 14195 Berlin (Germany)
E-mail: benesh.joseph@fu-berlin.de
Prof. Dr. R. Tampé
Institute of Biochemistry, Biocenter, Goethe University Frankfurt
Max-von-Laue-Str. 9, 60438 Frankfurt/Main (Germany)
E-mail: tampe@em.uni-frankfurt.de

[**] A previous version of this manuscript has been deposited on a preprint server (https://doi.org/10.26434/chemrxiv-2023-643mn).

Here we addressed the above challenges using pulsed electron-electron double resonance (PELDOR, also known as DEER) spectroscopy.[13] This technique allows for precise determination of distances between site-specifically engineered spin labels within a membrane protein, even in the cellular environment.[14] Such constraints can describe the large-scale conformational transitions and interdomain communications, even to atomistic details when sufficient distance constraints are determined.[15] Conventionally, PELDOR employs nitroxide (NO) spin labels and the methanethiosulfonate spin label (MTSL, which creates the side chain named R1) is the most preferred label for proteins. Other spin labels based on shielded nitroxides, Gd^{3+}, trityl and Cu^{2+} are increasingly being used for structural investigations, especially under native environments.[16] Here, we exploited the similar size and charge of the paramagnetic Mn^{2+} ions to replace the Mg^{2+} ions in presence of ATP.[1,17] Combining Mn^{2+} substitution with an engineered nitroxide label allowed us to simultaneously monitor ATP binding and the conformation at the two NBSs. Further, by introducing a nitroxide pair at the TMDs, we observed ATP binding and its effect on both the NBSs and the TMDs in the same sample. Though Mn^{2+} has been demonstrated as a useful tag for biomolecules, a concomitant Mn^{2+}–NO, Mn^{2+}–Mn^{2+}, and NO–NO distance measurement in the same sample has not been reported yet.[18] Even more, by performing such experiments in a time-resolved manner, we elucidated the differential role of the NBSs for the forward and reverse transitions. Though PELDOR holds great promise for time-resolved observation of biomolecular dynamics, its application to large membrane complexes is very challenging.[19] We exploited the thermophilic nature of TmrAB to resolve its dynamics by preparing samples at a lowered temperature. These multifaceted sets of experiments reveal that type IV ABC transporters might use catalytic asymmetry to regulate the kinetics of the conformational cycle.

Results and Discussion

Design and spin labeling of TmrAB cysteine variants

TmrAB transitions from an inward-facing (IF) to an outward-facing (OF) conformation upon ATP binding or vanadate trapping (see sample preparation in Supporting Information).[15b] This equilibrium transition is driven through an enthalpy-entropy compensation mechanism in a temperature independent manner over a broad range (30–60 °C).[20] Thus, different temperatures might adjust the extent of nucleotide binding/hydrolysis and the kinetics of the conformational transitions, but not alter the thermodynamic basis as such. Here, we engineered single-cysteine variants at the NBSs, where $A416C^A$ and $L458C^B$ variants probed distances to bound Mn^{2+}–ATP (Figure 1a). To probe the conformation using NO–NO PELDOR we used the $V288C^A$-$E272C^B$ variant for the TMDs and $A416C^A$-$L458C^B$ and $V461C^A$-$D349C^B$ variants for the NBSs. The $V288C^A$-$V461C^A$-$E272C^B$ variant was used to concurrently monitor both TMDs and NBSs using NO–NO, Mn^{2+}–NO, and Mn^{2+}–Mn^{2+} PELDOR (Figure 2a). All these variants actively hydrolyzed ATP and replacing Mg^{2+} with Mn^{2+} had little effect on the activity (Supplementary Figure S1). Typically, in vitro experiments with ABC transporters employ mM concentration of nucleotides. However, when Mg^{2+} is replaced with Mn^{2+}, such a large free Mn^{2+} concentration will induce fast relaxation of nitroxide labels, and distance measurements would become difficult or even impossible. Here we overcame this issue by a fast buffer-exchange step following incubation with Mn^{2+}–ATP.

Mn^{2+}–ATP is preferentially hydrolyzed at the c-NBS

At first, we determined distances between $A416R1^A$ and Mn^{2+}–ATP in TmrAB. As TmrAB exists in an equilibrium in presence of ATP,[15b] this experiment could yield four distances: distances to Mn^{2+}–ATP bound to the c-NBS and d-NBS in the IF (open NBSs) and OF (closed NBSs) conformations, respectively (green and purple dashed lines in Figure 1a). Simulations showed that the interspin distances can clearly differentiate Mn^{2+}–ATP bound between c-NBS and d-NBS. However, for both NBSs, the distances did not change appreciably when the NBSs close. We experimentally determined these distances using Mn^{2+}–NO PELDOR spectroscopy. This approach has earlier been used for model compounds, RNA and soluble proteins, but not yet for a membrane protein.[17a,18b–c,21] Briefly, incubation with Mn^{2+}–ATP was performed at 50 °C for 5 min, and the sample was transferred on ice afterwards. Subsequently, the buffer was rapidly exchanged with ice-cold buffer containing 10 mM ATP (and no Mg^{2+} or Mn^{2+}, unless otherwise specified) using a rapid gel-filtration centrifugation. PELDOR samples were prepared and immediately frozen in liquid nitrogen.

We observed only a single distance corresponding to the d-NBS (Figure 1c, for experimental reasons, we cannot quantify this fraction of the transporters). Thus, Mn^{2+} at the c-NBS is lost, likely due to ATP hydrolysis. To further verify this conclusion, we prepared another sample in the vanadate-trapped state, which stabilizes the NBSs in a Mn^{2+}–ADP–VO_4^{3-} state. Interestingly, the primary data revealed an additional distance, which corresponds to the c-NBS (also see Figure 1d). Thus, the c-NBS might rapidly hydrolyze ATP, whereas the d-NBS preferentially harbors an occluded ATP. Overall, the experimental data match rather well with the predicted distances, except that it cannot be concluded whether the Mn^{2+}–ATP binds to the open or closed conformation at the NBSs. The modulation depths for the Mn^{2+}–NO PELDOR ranged between 5–20 % (Figures 1–3). It could reach up to 30 % more under our experimental set up for a 100 %-labeled sample (pulse settings are given in Supporting Information Table 1). For MTSL, we obtained a good labeling efficiency (70–100 %). The decreased modulation we observed is mostly contributed by free manganese, which could not be totally removed during the gel-filtration step, and it somewhat varied between individual experiments. Importantly, this contribu-

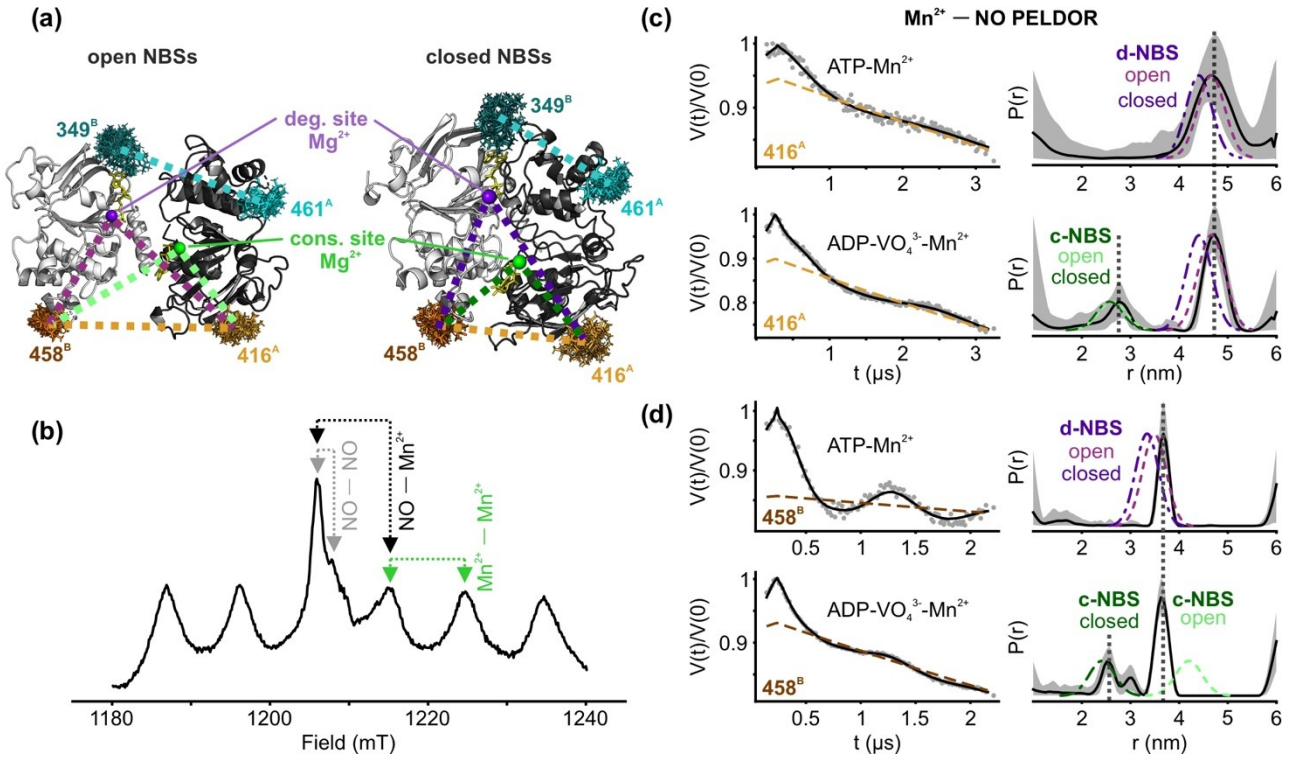

Figure 1. Mn^{2+}–ATP binding at the two NBSs. (a) MTSL labelled positions with the rotamers and Mg^{2+} ions are highlighted at the NBDs in the open or closed conformation. TmrA (black), TmrB (grey), Mg^{2+} (in green or purple), and ATP (yellow) are highlighted. (b) Echo-detected field sweep spectrum of MTSL labelled TmrAB with bound Mn^{2+}–ATP. The nitroxide spectrum overlaps with the Mn^{2+} central transition and the position of the pump and observer pulses for NO-NO, Mn^{2+}–NO, and Mn^{2+}–Mn^{2+} 4-pulse PELDOR at Q-band (34 GHz) are indicated. (c,d) Mn^{2+}–NO PELDOR data (left) and the corresponding distance distributions (right) obtained using the A416R1^{A} or L458R1^{B} variant as indicated (in black). A 95% confidence interval for the probability distance distributions is shown. The simulated distances on the IF and OF structures (PDBs 6RAG and 6RAJ respectively) are overlaid (in dotted lines). Simulations were performed using the MMM program and data were analyzed using the DeerLab platform.[12]

tion is identical for a particular sample set, which allows a quantitative comparison of modulation depths between those samples. Overall, the smaller modulation depths also effectively suppressed any multispin contribution for the relevant samples.[22]

As position A416R1^{A} cannot differentiate between open and closed conformations at the NBSs, we engineered another spin label at position L458C^{B}. Simulations showed that distances from L458R1^{B} can differentiate the two conformations at the c-NBS. As observed with C416R1, in presence of Mn^{2+}–ATP, L458R1 gave only a single distance corresponding to the d-NBS (Figure 1d). No distances were observed corresponding to the open or closed conformation at the c-NBS. In the vanadate-trapped state, we observed a second distance corresponding to the closed conformation of c-NBS. Thus, we did not observe any Mn^{2+}–ATP binding to the open conformation at the c-NBSs (and d-NBS as well, see Figure 2c). Cryo-EM structures suggested that nucleotides (ATP or ADP) can bind to both NBSs in the open conformation.[6] We could not observe this interaction, which is likely due to the differences in the experimental conditions. Open NBSs might have a reduced affinity for nucleotides and a large amount of ATP (as in the cryo-EM samples, which we cannot have as that would interfere with Mn^{2+}–NO PELDOR) would be necessary to observe this binding.

Concomitant observation of TMDs and NBSs: NO–NO and Mn^{2+}–NO PELDOR

For transporters with catalytic asymmetry, coupling between NBSs and TMDs during the transport cycle remains elusive.[7a,23] To further elucidate the mechanistic details, we designed an experiment to observe the conformation of both TMDs and NBSs within the same sample. We engineered a triple labeled TmrAB by combining the previously used V288C^{A}-E272C^{B} construct with the V461C^{A} substitution at the NBS (Figure 2a). Position V461C^{A} was chosen as simulations showed that it can clearly distinguish between open and closed conformations at the d-NBS (Figure 2c). This cysteine variant was labeled using MTSL with high efficiency (>70%) and is ATPase active (Supplementary Figure S1). We subsequently prepared samples as described earlier after incubating with Mn^{2+}–ATP. In this sample, the conformation of TMDs and NBSs was observed using NO–NO and Mn^{2+}–NO PELDOR, respectively. The nitroxide spin labels engineered on the TMDs and NBS are far

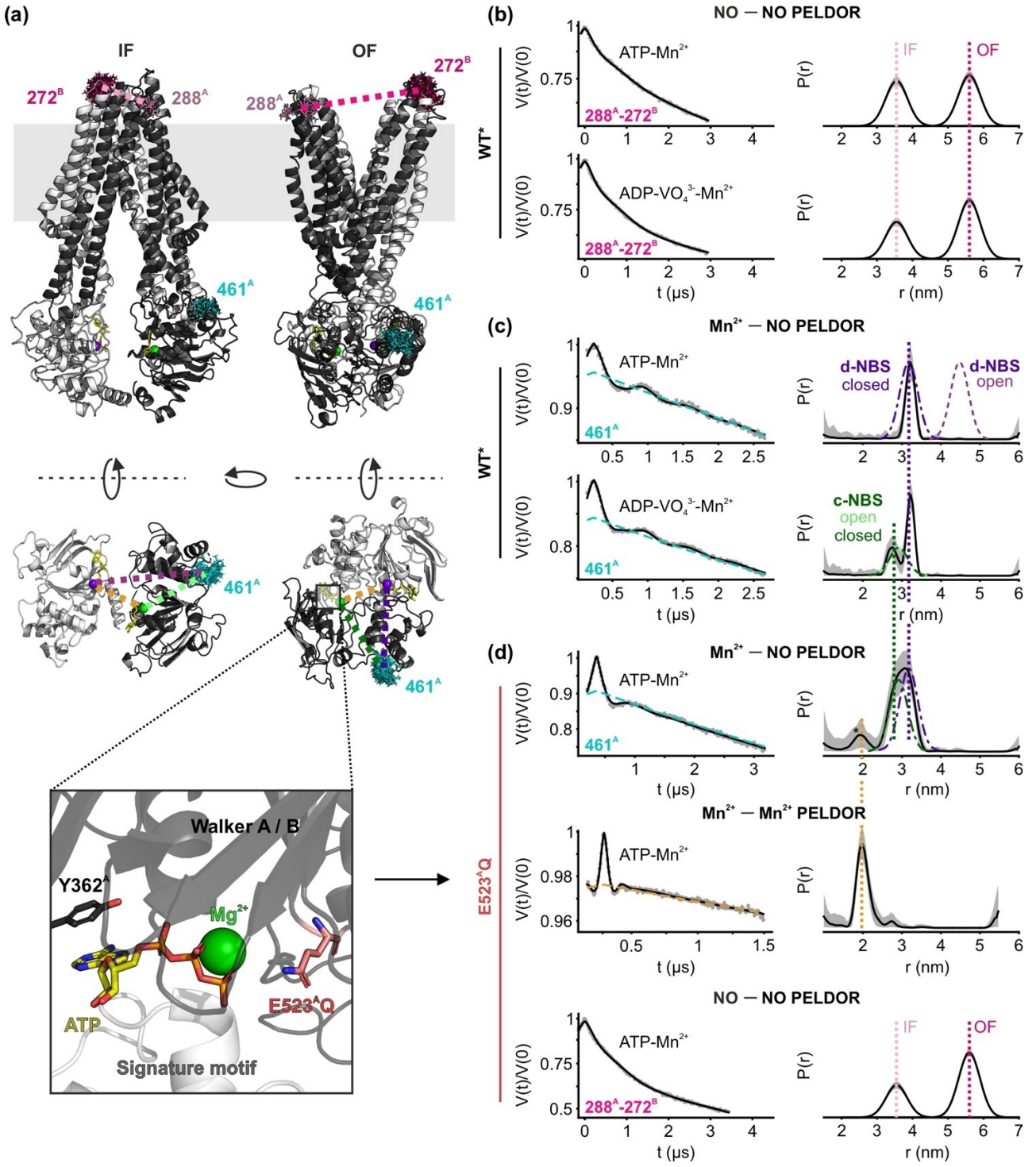

Figure 2. Concomitant Mn^{2+}–NO, NO–NO and Mn^{2+}–Mn^{2+} 4-pulse PELDOR of TmrAB at Q-band. (a) MTSL labeled positions and the Mg^{2+} ions are highlighted at the NBSs and TMDs in the IF and OF conformations. TmrA (black), TmrB (grey), Mg^{2+} (in green or purple), and ATP (yellow) are highlighted. (b,c,d) Left, NO–NO (for $V288R1^{A}$-$E272R1^{B}$, simulations are shown in Figure S3), Mn^{2+}–NO or Mn^{2+}–Mn^{2+} PELDOR data and the corresponding distance distributions (right) in the Cys-less (WT*) or the E-to-Q background (as highlighted at bottom in panel a). Simulations of Mn^{2+}–NO distances in the IF and OF conformations (PDBs 6RAG and 6RAJ respectively) are overlaid with dotted lines and the Mn^{2+}–Mn^{2+} distance is indicated with a vertical line (in orange). Data were analyzed using the DeerLab platform.[12] For $V288R1^{A}$-$E272R1^{B}$, an experimentally determined two Gaussian model corresponding to the IF (apo sample) and OF ($ADP–VO4^{3-}–Mg^{2+}$ sample) conformations was used for the analysis (Supplementary Figure S3c–d). A 95% confidence interval for the probability distance distributions is shown, which is invisible if thinner than the linewidth.

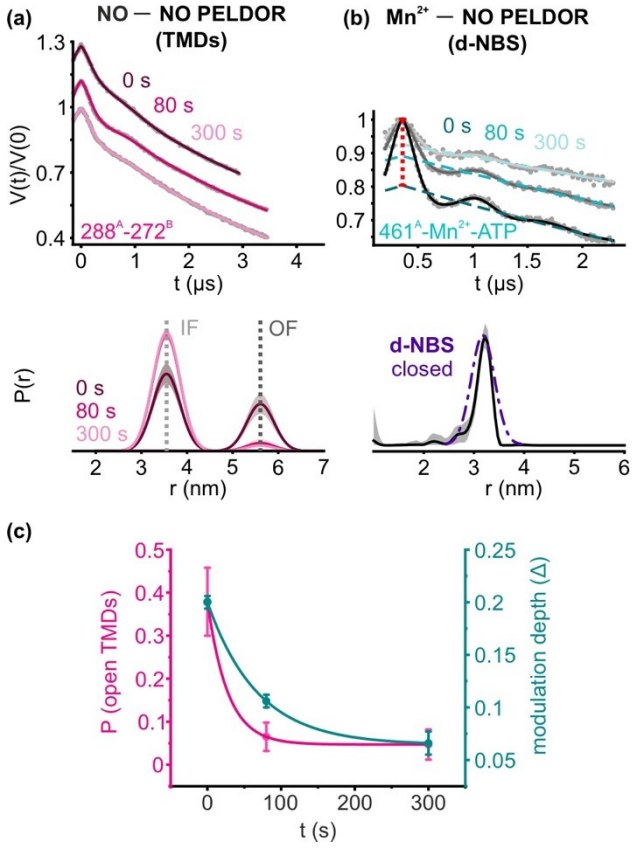

Figure 3. Reverse transition (OF-to-IF) in TmrAB. (a) Time resolved NO-NO (for V288R1^{A}-E272R1^{B}) or (b) Mn^{2+}–NO (using V461R1^{A}) 4-pulse PELDOR at Q-band and the corresponding distance distributions. (c) The variation of modulation depth (cyan) and the probability amplitude (magenta) of the distance distributions (for OF conformation) are plotted against time. Data were globally analyzed using the DeerLab platform.[12] For V288R1^{A}-E272R1^{B}, an experimentally determined two Gaussian model was used for the analysis as described for Figure 2 (see Supplementary Figure S3c). A 95% confidence interval is shown, which is invisible if thinner than the linewidth.

separated ($\geq$8–12 nm) and their interaction was too weak to be detected within the observable time window of the PELDOR data (Supplementary Figure S2).

First, we determined distances for samples incubated with Mn^{2+}–ATP. At the TMDs, NO–NO PELDOR revealed a mixed population between open and closed conformations (Figure 2b). For the NBSs, Mn^{2+}–NO PELDOR gave only a single distance corresponding to the closed conformation at the d-NBS (Figure 2c). Yet, it is difficult to conclude that the fraction of open TMDs corresponds exclusively to the closed population of the d-NBS, as the c-NBS also could be in a closed state, but without Mn^{2+} (in a Mn^{2+} free post-hydrolytic state). The absence of distances corresponding to the open d-NBS conformation reveals a reduced affinity for ATP in this conformation (as with c-NBS, Figure 1d). Next, we performed similar experiments with vanadate trapped (5 min at 50 °C) TmrAB (Figure 2b–c, ADP–VO_4^{3-}–Mg^{2+}). NO–NO PELDOR revealed an enhanced population of the OF conformation at the TMDs. This is accompanied with the presence of additional distances for the Mn^{2+}–NO PELDOR, corresponding to the closed conformation of the c-NBS (also see Figure 1c).

Having consistently observed only a small population corresponding to the closed c-NBS (Figure 1c–d and 2c), we repeated the above experiments after substituting the conserved Walker-B catalytic glutamate to glutamine (E523-to-Q523) at the c-NBS. This substitution significantly reduces the ATPase activity.[24] The NO–NO PELDOR of this sample revealed an increased fraction of transporters having TMDs in the OF conformation (Figure 2b vs. 2d, NO-NO PELDOR). Remarkably, Mn^{2+}–ATP binding was substantially increased in this variant. The amplitude of the probability distribution for Mn^{2+}(–ATP) bound to the c-NBS became nearly equal to the contribution from the d-NBS Figure 2d). Thus, the E-to-Q mutation leads to a stable occlusion of Mn^{2+}–ATP at the c-NBS and the drastically decreased ATP hydrolysis leads to a larger fraction of TmrAB being trapped in the OF conformation. The Mn^{2+}–NO PELDOR suggested the presence of a small peak at $\approx$2 nm, which agrees with the simulation for Mn^{2+}–Mn^{2+} distances. We further characterized this distance using Mn^{2+}–Mn^{2+} PELDOR on the same sample, which confirmed the presence of two Mn^{2+} atoms at the NBSs of the E-to-Q variant (Figure 2d, Mn^{2+}–Mn^{2+} PELDOR).

Reverse (OF-to-IF) transition correlates with loss of Mn^{2+}–ATP from the d-NBS

To delineate the relative role of the two NBSs, we preformed additional experiments with the triple-labeled variant. TmrAB exhibits maximal ATPase and transport activities at ~68 °C.[4a,5] At lower temperatures, the amplitude and rate of transition is significantly reduced (into the range of several minutes). We exploited this possibility to prepare samples in a time-resolved manner and to follow the correlated changes for equilibrium populations between the TMDs and NBSs using NO–NO and Mn^{2+}–NO PELDOR spectroscopy. Briefly, samples were incubated with Mn^{2+}–ATP (10 mM each) for 5 min at 50 °C and transferred to ice. Protein was immediately gel-filtrated to remove free ATP and Mn^{2+} using ice-cold buffers and the eluate was moved to ice. At this point, samples were transferred to preheated ESR tubes at 50 °C and incubated for different durations up to 5 min and snap frozen in liquid nitrogen. Due to the absence of external ATP, the system might undergo a single reverse (OF-to-IF) transition during the incubation. The conformational transitions in TmrAB are strongly temperature-dependent, revealing large energy barriers between different states. In agreement, prolonged incubation at 4 °C or a transfer to 4 °C following incubation at a higher temperature does not alter the equilibrium population (Supplementary Figure S3). The NO–NO PELDOR (at V288R1^{A}-E272R1^{B}) of the time zero sample revealed a mixed population at the TMDs as before (Figure 3a). Remarkably, the amount of this OF population was reduced over time towards a small fraction within 80–300 s. We further monitored the NBSs using Mn^{2+}–NO

PELDOR. As expected from earlier observations (Figures 1c and 2c), it gave a single distance (3.20 ± 0.15 nm, Figure 3b), corresponding to the closed d-NBS (and a quantitative correlation of this population with TMDs is not possible for experimental reasons). Here, the conformation of the c-NBS cannot be deduced except for the lack of Mn^{2+}. Having these samples prepared in an identical manner, the modulation depth of these PELDOR data provides a quantitative information on the presence of Mn^{2+}–ATP at the d-NBS. ATP hydrolysis or dissociation would result in the loss of Mn^{2+} and thereby decrease of modulation depth. Interestingly, correlated with the change (closure) in the probability amplitudes of the distances at the TMDs, the modulation depth decreased over time (Figure 3c). Overall, in the observed fraction of the TMDs, OF-to-IF transition is accompanied with dissociation of Mn^{2+}–ATP, most likely through opening of the d-NBS.

Reverse transition involves opening of both NBSs and is accelerated by the presence of Mg^{2+}, ADP, or substrate

To further elucidate the relative conformation of the TMDs and the NBSs, we prepared independent sets of samples for both NBSs and the TMDs. Initially, we followed the forward (IF-to-OF) transition in presence of excess ATP + EDTA (50 mM and 0.5 mM, respectively) using the V288R1^{A}-E272R1^{B} variant. TmrAB gradually shifted towards the OF conformation reaching a ≈60:40 (OF:IF) population in 5 min at 50 °C. At this point free ATP–EDTA was removed by desalting (at 4 °C, in presence of various ligands as indicated) and the sample was transferred to ice. Subsequently, the reverse transition (OF-to-IF) was monitored in the presence of EDTA (0.5 mM, to chelate any residual Mg^{2+}), ADP (1 mM), substrate (K5F, which is the fluorophore labeled peptide RRYC(K^{Fluorescein})STEL, 50 µM), or Mg^{2+} (50 mM). In the absence of any ligands (+EDTA sample), the TMDs returned to the IF conformation at a much slower rate (Figure 4a, black circles and Supplementary Figures S4). Surprisingly, in the presence of excess Mg^{2+}, transition was enhanced and the TMDs almost

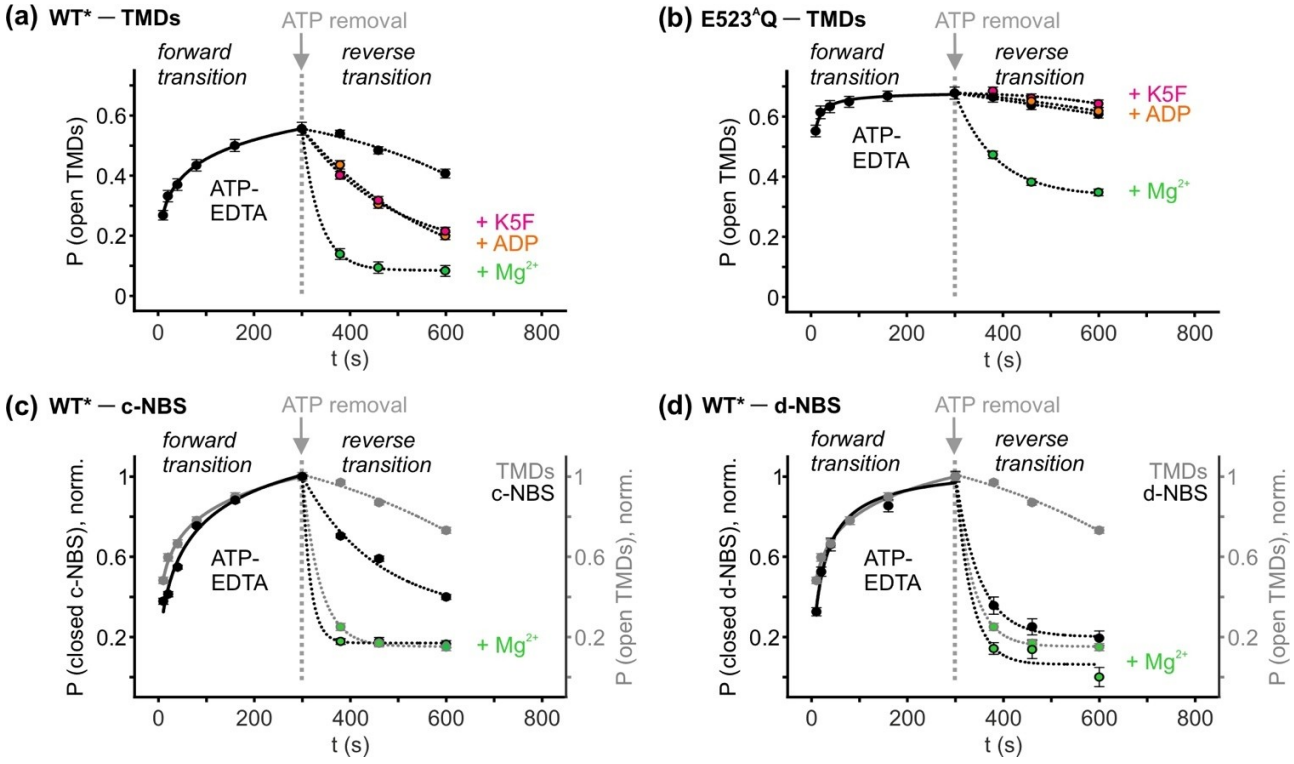

Figure 4. Forward (IF-to-OF) and reverse transition (OF-to-IF) in TmrAB and the effect of ADP, substrate (K5F) or Mg^{2+}. (a–b) Time-resolved NO–NO 4-pulse PELDOR was performed on the V288R1^{A}-E272R1^{B} variant at the TMDs in the Cys-less (WT*) or E-to-Q background at Q-band and the distances were determined under different conditions as indicated. (c,d) Forward and reverse transitions at the consensus (A416R1^{A}-L458R1^{B}) and degenerate NBS (V461R1^{A}-D349R1^{B}, denoted as c-NBS and d-NBS, respectively) and data for the TMDs (from panel a) are overlaid. Data were analyzed using the DeerLab platform and normalized probability amplitudes are shown for a qualitative comparison. For V288R1^{A}-E272R1^{B}, A416R1^{A}-L458R1^{B} and V461C^{A}-D349C^{B}, an experimentally determined model corresponding to the IF (apo sample) and OF (ADP–VO_4^{3-}–Mg^{2+} sample) conformations was used for the analysis (see Supplementary Figures S3c–d, S4–S7). The phase memory time (T_M) of the spin labels between the open and closed conformations for the TMDs and the two NBSs were the same (data not shown). Error bars show 95% confidence interval.

completely resorted to the closed conformation (Figure 4a, green circles).

We further reasoned that if ATP negatively regulates opening of the d-NBS, the presence of an excess of ADP might have an enhancing effect. As expected, addition of ADP (1 mM) considerably accelerated the transition (Figure 4a, orange circles). Strikingly, a peptide substrate (K5F) also had a similar effect on the reverse transition (Figure 4a, magenta circles). While the effect of ADP could be explained through a competitive replacement of ATP, enhancement by substrate is a surprising observation. This might involve an interaction of the substrate in a post-hydrolysis conformation, which might stabilize the high affinity IF conformation. Notably, in the E-to-Q variant, K5F and ADP had little effect (Figure 4b and Supplementary Figure S5), implying that they interact in a post-hydrolytic state. Strikingly, the forward transition was accelerated, and the reverse transition was significantly reduced in the E-to-Q variant, revealing a significant alteration of the energy landscape. The residual ATPase activity of this variant might drive the partial reversal in presence of Mg^{2+}, thereby further confirming that ATP hydrolysis is necessary to accelerate the reverse transition.

Considering the severely decreased ATPase activity of the d-NBS, such a strong effect of Mg^{2+} suggested an important role played by the c-NBS. To deduce the conformation of the NBSs, we performed identical experiments on them and compared with the TMDs. As these are independent experiments on different cysteine variants, we limited the analysis towards a more qualitative comparison by normalizing the observed probability amplitudes. For both NBSs, reverse transition (opening) was slower in the absence of Mg^{2+} and appeared to be faster than the corresponding change (closure) for the TMDs, which is rather unlikely (Figure 4c–d and Supplementary Figures S6–S7). These differences might be accounted by the variation between the corresponding sample sets (spin labeling at different positions and possible variation in the residual amounts of ATP and or Mg^{2+} following desalting etc.). Most importantly, in presence of Mg^{2+}, both NBSs fully reversed (opened) in perfect correlation with the closure of the TMDs. The c-NBS variant appears to open faster than the d-NBS in presence of Mg^{2+} and a more advanced sample preparation set up would help to further resolve this transition.

Conclusion

Here, we addressed the functional relevance of catalytic asymmetry in ABC exporters using advanced ESR spectroscopy techniques combined with tailored samples preparation protocols. At high ATP concentrations, we observed an equilibrium between IF and OF conformations. The d-NBS showed consistent Mn^{2+}–ATP binding, whereas at the c-NBS Mn^{2+}–ATP was detectable only upon vanadate trapping or in the catalytically impaired E-to-Q variant (Figures 1–3). However, from independent experiments we found that a comparable fraction of the c-NBS as well is closed under similar conditions (Figure 4c, forward transition, samples up to at 300 s). Therefore, preferential ATP hydrolysis at the c-NBS might lead to an immediate release of Mn^{2+} (and possibly P_i), which in effect made the closed c-NBS conformation invisible in our Mn^{2+}–NO PELDOR experiments (Figure 5, step 3). Based on the cryo-EM structures and molecular dynamic simulations of TmrAB, such a path for release of P_i has been identified earlier.[6] The pronounced enhancement of reverse transition by Mg^{2+}/Mn^{2+} as well as its inhibition in the E-to-Q variant (Figures 3–4) reveal that ATP hydrolysis at the c-NBS must be the first step to initiate reverse transition.

For ABC transporters with asymmetric NBSs, two unique intermediate states, which are structurally yet uncharacterized, have been suggested. Preferential ATP hydrolysis at the c-NBS would create an OF transporter with partially/fully open c-NBS and closed d-NBS.[7a] This intermediate state may transition to an IF conformation with the d-NBS remaining fully or partially closed while the c-NBS is open.[7a,23b] Cryo-EM structures revealed two additional structures for TmrAB; two asymmetric unlocked-return (UR) conformations, which are similar to the OF-

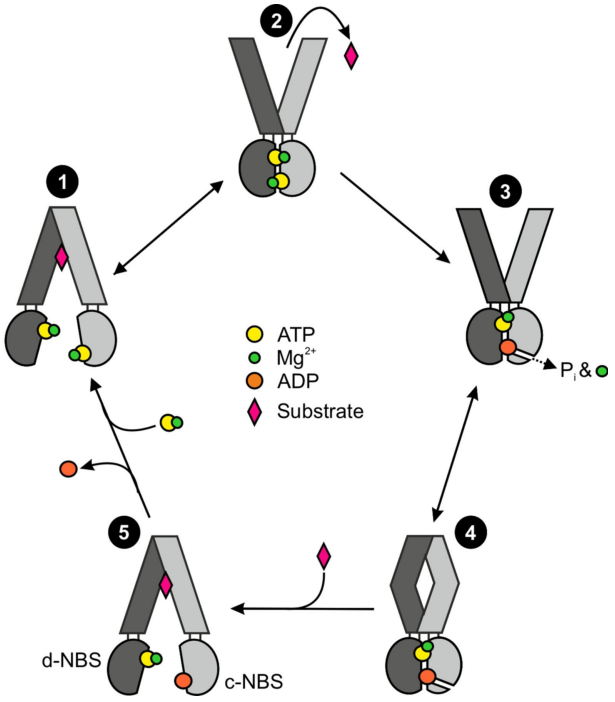

Figure 5. Mechanism for substrate translocation in TmrAB. Substrate binds to the high affinity IF conformation (1) and ATP binding induces transition to the OF conformation and release of substrate from the low affinity binding pocket (2). This is followed by ATP hydrolysis at the c-NBS (3) and immediate release of P_i and Mg^{2+} through a previously identified path in the closed conformation[6] (3). The TMDs may also adopt to an occluded conformation (4) and further transition to the IF conformation (5). This step might be regulated through opening and loss of ATP from the d-NBS. This reverse transition (towards IF conformation) is accelerated in presence of ADP, substrate and most significantly under hydrolyzing conditions. Subsequently, substrate binds to the IF conformation and replacement of Mg^{2+}–ADP with Mg^{2+}–ATP resets the cycle to begin the next round of transport.

occluded conformation with a slightly separated NBD interface.[6] For TmrAB, we are unable to unambiguously assign either of these conformations from the spectroscopic data. We observed that Mn^{2+}(–ATP) is gradually lost from the d-NBS when the TMDs reversed to the closed (IF) conformation (Figure 3c), which should be associated with an opening of this NBS (Figure 4d, Mg^{2+} sample). Further, a correlated movement between the two NBSs and TMDs (Figure 4c–d) shows that both NBSs completely open during reverse transition of the TMDs to the closed conformation under the experimental conditions.

In type IV ABC transporters, ATP binding might be the power stroke for forward (IF-to-OF) transition and release of the substrate after its translocation.[23a,24a,25] Under non-hydrolyzing conditions, the reverse transition is extremely slow (Figure 4a). Our results shows that ATP hydrolysis at the c-NBS is the trigger to accelerate reverse transition (Figure 2d, 4a–b). This might create an intermediate state, which fully reverses towards the IF conformation with an accelerated rate (Figure 4c–d, Figure 5, step 3). Having a drastically reduced ATPase activity, the d-NBS stably binds ATP, (Figures 1–2). This in effect prevents complete opening of (both) NBS and thereby might regulate the overall kinetics of reverse transition (Figure 5, transition between steps 3 to 5). This may increase the lifetime of the OF conformation and allows substrate to be release from the low-affinity binding pocket. Further, this would minimize futile ATPase cycles in the absence of substrate. The overall equilibrium might be regulated through an interplay between Mg^{2+}–ATP, Mg^{2+}–ADP, and substrate concentrations as well as the rates for forward and reverse transitions. Following the forward and reverse kinetics under different conditions would provide further insights into this regulatory mechanism, which is beyond the scope of this study. Our observations might provide a general explanation for the functional role of asymmetric NBSs and the spectroscopic approach presented here offers a potential tool to further explore catalytic (a)symmetry in related ABC transporters.

Acknowledgements

This work was financially supported from the Deutsche Forschungsgemeinschaft via the Emmy Noether program (JO 1428/1-1) to B.J., SFB 1507—"Membrane-associated Protein Assemblies, Machineries, and Supercomplexes" to R.T. and B.J., and a large equipment fund (438280639) to B.J. M.R. and B.J. acknowledges the generous support from Goethe University Frankfurt. Open Access funding enabled and organized by Projekt DEAL.

Conflict of Interest

The authors declare no conflict of interest.

Data Availability Statement

The data that support the findings of this study are available from the corresponding author upon reasonable request.

Keywords: ABC Transporter · EPR Spectroscopy · Manganese · Nucleotide-Binding Sites · Spin Labels

[1] a) T. Wiegand, D. Lacabanne, K. Keller, R. Cadalbert, L. Lecoq, M. Yulikov, L. Terradot, G. Jeschke, B. H. Meier, A. Bockmann, *Angew. Chem. Int. Ed.* **2017**, *56*, 3369–3373; b) A. Collauto, S. Mishra, A. Litvinov, H. S. McHaourab, D. Goldfarb, *Structure* **2017**, *25*, 1264–1274.

[2] a) A. L. Davidson, E. Dassa, C. Orelle, J. Chen, *Microbiol. Mol. Biol. Rev.* **2008**, *72*, 317–364; b) D. J. Slotboom, T. W. Ettema, M. Nijland, C. Thangaratnarajah, *FEBS Lett.* **2020**, *594*, 3898–3907.

[3] a) C. Thomas, R. Tampé, *Annu. Rev. Biochem.* **2020**, *89*, 605–636; b) K. P. Locher, *Nat. Struct. Mol. Biol.* **2016**, *23*, 487–493.

[4] a) A. Zutz, J. Hoffmann, U. A. Hellmich, C. Glaubitz, B. Ludwig, B. Brutschy, R. Tampé, *J. Biol. Chem.* **2011**, *286*, 7104–7115; b) C. Thomas, S. G. Aller, K. Beis, E. P. Carpenter, G. Chang, L. Chen, E. Dassa, M. Dean, F. Duong Van Hoa, D. Ekiert, R. Ford, R. Gaudet, X. Gong, I. B. Holland, Y. Huang, D. K. Kahne, H. Kato, V. Koronakis, C. M. Koth, Y. Lee, O. Lewinson, R. Lill, E. Martinoia, S. Murakami, H. W. Pinkett, B. Poolman, D. Rosenbaum, B. Sarkadi, L. Schmitt, E. Schneider, Y. Shi, S. L. Shyng, D. J. Slotboom, E. Tajkhorshid, D. P. Tieleman, K. Ueda, A. Varadi, P. C. Wen, N. Yan, P. Zhang, H. Zheng, J. Zimmer, R. Tampé, *FEBS Lett.* **2020**, *594*, 3767–3775.

[5] A. Nöll, C. Thomas, V. Herbring, T. Zollmann, K. Barth, A. R. Mehdipour, T. M. Tomasiak, S. Bruchert, B. Joseph, R. Abele, V. Olieric, M. Wang, K. Diederichs, G. Hummer, R. M. Stroud, K. M. Pos, R. Tampé, *Proc. Natl. Acad. Sci. USA* **2017**, *114*, E438–E447.

[6] S. Hofmann, D. Januliene, A. R. Mehdipour, C. Thomas, E. Stefan, S. Bruchert, B. T. Kuhn, E. R. Geertsma, G. Hummer, R. Tampé, A. Moeller, *Nature* **2019**, *571*, 580–583.

[7] a) T. Stockner, R. Gradisch, L. Schmitt, *FEBS Lett.* **2020**, *594*, 3815–3838; b) R. Dastvan, S. Mishra, Y. B. Peskova, R. K. Nakamoto, H. S. McHaourab, *Science* **2019**, *364*, 689–692.

[8] J. A. Olsen, A. Alam, J. Kowal, B. Stieger, K. P. Locher, *Nat. Struct. Mol. Biol.* **2020**, *27*, 62–70.

[9] a) M. Hohl, L. M. Hurlimann, S. Bohm, J. Schoppe, M. G. Grutter, E. Bordignon, M. A. Seeger, *Proc. Natl. Acad. Sci. USA* **2014**, *111*, 11025–11030; b) T. M. Thaker, S. Mishra, W. Zhou, M. Mohan, Q. Tang, J. D. Faraldo-Gomez, H. S. McHaourab, T. M. Tomasiak, *Nat. Chem. Biol.* **2022**, *18*, 226–235; c) M. L. Oldham, R. K. Hite, A. M. Steffen, E. Damko, Z. Li, T. Walz, J. Chen, *Nature* **2016**, *529*, 537–540; d) L. Wang, Z. L. Johnson, M. R. Wasserman, J. Levring, J. Chen, S. Liu, *eLife* **2020**, *9*, e56451; e) F. Liu, Z. Zhang, L. Csanady, D. C. Gadsby, J. Chen, *Cell* **2017**, *169*, 85–95.

[10] a) S. Mishra, B. Verhalen, R. A. Stein, P. C. Wen, E. Tajkhorshid, H. S. McHaourab, *eLife* **2014**, *3*, e02740; b) K. Goda, Y. Donmez-Cakil, S. Tarapcsak, G. Szaloki, D. Szollosi, Z. Parveen, D. Turk, G. Szakacs, P. Chiba, T. Stockner, *PLoS Genet.* **2020**, *16*, e1009016.

[11] a) L. Fábregas Ibáñez, G. Jeschke, S. Stoll, *Magn. Reson.* **2020**, *1*, 209–224; b) G. Jeschke, *Protein Sci.* **2021**, *30*, 125–135.

[12] a) C. Basso, P. Vergani, A. C. Nairn, D. C. Gadsby, *J. Gen. Physiol.* **2003**, *122*, 333–348; b) K. Szabó, G. Szakács, T. Hegedüs, B. Sarkadi, *J. Biol. Chem.* **1999**, *274*, 12209–12212.

[13] a) O. Schiemann, C. A. Heubach, D. Abdullin, K. Ackermann, M. Azarkh, E. G. Bagryanskaya, M. Drescher, B. Endeward, J. H. Freed, L. Galazzo, D. Goldfarb, T. Hett, L. Esteban Hofer, L. Fabregas Ibanez, E. J. Hustedt, S. Kucher, I. Kuprov, J. E. Lovett, A. Meyer, S. Ruthstein, S. Saxena, S. Stoll, C. R. Timmel, M. Di Valentin, H. S. McHaourab, T. F. Prisner, B. E. Bode, E. Bordignon, M. Bennati, G. Jeschke, *J. Am. Chem. Soc.* **2021**, *143*, 17875–17890; b) M. Pannier, S. Veit, A. Godt, G. Jeschke, H. W. Spiess, *J. Magn. Reson.* **2000**, *142*, 331–340.

[14] a) D. Goldfarb, *Curr. Opin. Struct. Biol.* **2022**, *75*, 102398; b) G. Jeschke, *Annu. Rev. Phys. Chem.* **2012**, *63*, 419–446; c) E. Bordignon, S. Bleicken, *Biochim. Biophys. Acta Biomembr.* **2018**, *1860*, 841–853; d) B. Joseph, A. Sikora, E. Bordignon, G. Jeschke, D. S. Cafiso, T. F. Prisner, *Angew. Chem. Int. Ed.* **2015**, *54*, 6196–6199; e) B. Joseph, A. Sikora, D. S. Cafiso, *J. Am. Chem. Soc.* **2016**, *138*, 1844–1847; f) P. P. Borbat, E. R. Georgieva, J. H. Freed, *J. Phys. Chem. Lett.* **2013**, *4*, 170–175; g) C. E. Tait, S. Stoll, *Phys. Chem. Chem. Phys.* **2016**, *18*, 18470–18485.

[15] a) Y. N. Chang, E. A. Jaumann, K. Reichel, J. Hartmann, D. Oliver, G. Hummer, B. Joseph, E. R. Geertsma, *Nat. Commun.* **2019**, *10*, 2032; b) K. Barth, S. Hank, P. E. Spindler, T. F. Prisner, R. Tampé, B. Joseph, *J. Am. Chem. Soc.* **2018**, *140*, 4527–4533; c) D. Sala, D. Del Alamo, H. S. McHaourab, J. Meiler, *Structure* **2022**, *30*, 1157–1168 e1153; d) A. Gopinath, B. Joseph, *Angew. Chem. Int. Ed.* **2022**, *61*, e202113448; e) D. Hilger, Y. Polyhach, E. Padan, H. Jung, G. Jeschke, *Biophys. J.* **2007**, *93*, 3675–3683.

[16] a) Y. Yang, F. Yang, Y. J. Gong, J. L. Chen, D. Goldfarb, X. C. Su, *Angew. Chem. Int. Ed.* **2017**, *56*, 2914–2918; b) T. F. Cunningham, M. R. Putterman, A. Desai, W. S. Horne, S. Saxena, *Angew. Chem. Int. Ed.* **2015**, *54*, 6330–6334; c) B. Joseph, V. M. Tormyshev, O. Y. Rogozhnikova, D. Akhmetzyanov, E. G. Bagryanskaya, T. F. Prisner, *Angew. Chem. Int. Ed.* **2016**, *55*, 11538–11542; d) G. Karthikeyan, A. Bonucci, G. Casano, G. Gerbaud, S. Abel, V. Thome, L. Kodjabachian, A. Magalon, B. Guigliarelli, V. Belle, O. Ouari, E. Mileo, *Angew. Chem. Int. Ed.* **2018**, *57*, 1366–1370; e) J. L. Wort, K. Ackermann, A. Giannoulis, A. J. Stewart, D. G. Norman, B. E. Bode, *Angew. Chem. Int. Ed.* **2019**, *58*, 11681–11685; f) N. Fleck, C. A. Heubach, T. Hett, F. R. Haege, P. P. Bawol, H. Baltruschat, O. Schiemann, *Angew. Chem. Int. Ed.* **2020**, *59*, 9767–9772; g) M. D. S. Ketter, O. Rogozhnikova, S. A. Dobrynin, V. M. Tormyshev, E. G. Bagryanskaya, B. Joseph, *J. Magn. Reson. Open* **2022**, *10–11*, 100041; h) S. Ketter, B. Joseph, *J. Am. Chem. Soc.* **2023**, *145*, 960–966; i) L. Hofmann, S. Ruthstein, *J. Phys. Chem. B* **2022**, *126*, 7486–7494; j) V. M. Tormyshev, A. S. Chubarov, O. A. Krumkacheva, D. V. Trukhin, O. Y. Rogozhnikova, A. S. Spitsyna, A. A. Kuzhelev, V. V. Koval, M. V. Fedin, T. S. Godovikova, M. K. Bowman, E. G. Bagryanskaya, *Chem. Eur. J.* **2020**, *26*, 2705–2712; k) T. S. Braun, P. Widder, U. Osswald, L. Gross, L. Williams, M. Schmidt, I. Helmle, D. Summerer, M. Drescher, *ChemBioChem* **2020**, *21*, 958–962; l) Z. Hasanbasri, K. Singewald, T. D. Gluth, B. Driesschaert, S. Saxena, *J. Phys. Chem. B* **2021**, *125*, 5265–5274.

[17] a) A. Giannoulis, A. Feintuch, T. Unger, S. Amir, D. Goldfarb, *J. Phys. Chem. Lett.* **2021**, *12*, 12235–12241; b) H. Kaur, B. Abreu, D. Akhmetzyanov, A. Lakatos-Karoly, C. M. Soares, T. Prisner, C. Glaubitz, *J. Am. Chem. Soc.* **2018**, *140*, 14112–14125.

[18] a) Z. Y. Wu, A. Feintuch, A. Collauto, L. A. Adams, L. Aurelio, B. Graham, G. Otting, D. Goldfarb, *J. Phys. Chem. Lett.* **2017**, *8*, 5277–5282; b) I. Kaminker, M. Bye, N. Mendelman, K. Gislason, S. T. Sigurdsson, D. Goldfarb, *Phys. Chem. Chem. Phys.* **2015**, *17*, 18197–18197; c) A. Meyer, O. Schiemann, *J. Phys. Chem. A* **2016**, *120*, 3463–3472; d) D. Akhmetzyanov, J. Plackmeyer, B. Endeward, V. Denysenkov, T. F. Prisner, *Phys. Chem. Chem. Phys.* **2015**, *17*, 6760–6766.

[19] a) A. Collauto, H. A. DeBerg, R. Kaufmann, W. N. Zagotta, S. Stoll, D. Goldfarb, *Phys. Chem. Chem. Phys.* **2017**, *19*, 15324–15334; b) T. Hett, T. Zbik, S. Mukherjee, H. Matsuoka, W. Bonigk, D. Klose, C. Rouillon, N. Brenner, S. Peuker, R. Klement, H. J. Steinhoff, H. Grubmuller, R. Seifert, O. Schiemann, U. B. Kaupp, *J. Am. Chem. Soc.* **2021**, *143*, 6981–6989; c) S. Maity, B. D. Price, C. B. Wilson, A. Mukherjee, M. Starck, D. Parker, M. Z. Wilson, J. E. Lovett, S. Han, M. S. Sherwin, *Angew. Chem. Int. Ed.* **2023**, *62*, e202212832.

[20] K. Barth, M. Rudolph, T. Diederichs, T. F. Prisner, R. Tampé, B. Joseph, *J. Phys. Chem. Lett.* **2020**, *11*, 7946–7953.

[21] D. Akhmetzyanov, P. Schops, A. Marko, N. C. Kunjir, S. T. Sigurdsson, T. F. Prisner, *Phys. Chem. Chem. Phys.* **2015**, *17*, 24446–24451.

[22] a) S. Valera, K. Ackermann, C. Pliotas, H. Huang, J. H. Naismith, B. E. Bode, *Chem. Eur. J.* **2016**, *22*, 4700–4703; b) T. von Hagens, Y. Polyhach, M. Sajid, A. Godt, G. Jeschke, *Phys. Chem. Chem. Phys.* **2013**, *15*, 5854–5866.

[23] a) C. A. J. Hutter, M. H. Timachi, L. M. Hurlimann, I. Zimmermann, P. Egloff, H. Göddeke, S. Kucher, S. Stefanic, M. Karttunen, L. V. Schafer, E. Bordignon, M. A. Seeger, *Nat. Commun.* **2019**, *10*, 2260; b) A. Harris, M. Wagner, D. Du, S. Raschka, L. M. Nentwig, H. Gohlke, S. H. J. Smits, B. F. Luisi, L. Schmitt, *Nat. Commun.* **2021**, *12*, 5254; c) H. Göddeke, M. H. Timachi, C. A. J. Hutter, L. Galazzo, M. A. Seeger, M. Karttunen, E. Bordignon, L. V. Schäfer, *J. Am. Chem. Soc.* **2018**, *140*, 4543–4551; d) A. Tóth, A. Janaszkiewicz, V. Crespi, F. Di Meo, *Commun. Biol.* **2023**, *6*, 149.

[24] a) E. Stefan, S. Hofmann, R. Tampé, *eLife* **2020**, *9*, e55943; b) E. Stefan, R. Obexer, S. Hofmann, K. Vu Huu, Y. Huang, N. Morgner, H. Suga, R. Tampé, *eLife* **2021**, *10*, e67732.

[25] H. Göddeke, L. V. Schäfer, *J. Am. Chem. Soc.* **2020**, *142*, 12791–12801.

Manuscript received: May 19, 2023
Accepted manuscript online: July 17, 2023
Version of record online: August 7, 2023